Personalized Computational Modeling Identifies Embolic Stroke of Undetermined Source Patients with Potential Arrhythmic Substrate

Savannah F. Bifulco,[1] Griffin D. Scott,[1] Sakher Sarairah,[2] Zeinab Birjandian,[2,5]

Caroline H. Roney,[3] Steven A. Niederer,[3] Christian Mahnkopf,[4] Peter Kuhnlein,[4]

Marcel Mitlacher,[4] David Tirschwell,[5] W. T. Longstreth Jr,[5,6] Nazem Akoum,[2] Patrick M. Boyle[1,7,8*]*

1: Department of Bioengineering, University of Washington, Seattle, WA, USA.

2: Division of Cardiology, University of Washington, Seattle, WA, USA.

3: School of Biomedical Engineering and Imaging Sciences, King's College London, London, UK.

4: Department of Cardiology, Klinikum Coburg, Coburg, Germany.

5: Department of Neurology, University of Washington, Seattle, WA, USA.

6: Department of Epidemiology, University of Washington, Seattle, WA, USA.

7: Institute for Stem Cell and Regenerative Medicine, University of Washington, Seattle, WA, USA.

8: Center for Cardiovascular Biology, University of Washington, Seattle, WA, USA.

***: Corresponding authors:**

PM Boyle; email: pmjboyle@uw.edu; mail: Foege N310H UW Mailbox 355061, Seattle WA 98195, USA; OR, N Akoum; email: nakoum@cardiology.washington.edu; mail: 1959 N Pacific St, Seattle WA 98115, USA

Word count, excluding Materials and Methods, References, and Figure Legends: 4342

Competing Interests: None declared

Abstract

Late-gadolinium enhanced (LGE)-MRI has revealed atrial fibrotic remodeling in embolic stroke of undetermined source (ESUS) patients comparable to that observed in atrial fibrillation (AFib) patients. Here, we use computational modeling to understand why fibrosis in ESUS does not cause arrhythmia. Left atrial (LA) models were reconstructed via a standardized process and simulations were conducted to probe the fibrotic substrate's capacity to sustain reentrant drivers (RD). RD-perpetuated arrhythmia was observed in 23/45 (51%) ESUS and 28/45 (62%) AFib models. LA models in which RDs were inducible had significantly more fibrosis than those which were non-inducible (16.8±5.04% vs. 10.19±3.14%; P<0.0001); however, between the specific subsets of inducible ESUS and AFib models, there was no difference in fibrosis burden (P=0.068). Thus, within our modeling framework, pro-arrhythmic properties of fibrosis in ESUS and AFib are indistinguishable, suggesting many ESUS patients have latent fibrotic substrate that may be a potential future source of arrhythmogenicity.

Introduction

Atrial fibrillation (AFib) is the most common cardiac arrhythmia, affecting 1-2% of the world's population and significantly contributing to worldwide morbidity and mortality (1). The primary source of AFib-related mortality is stroke, with around 20% of all ischemic strokes occurring in AFib patients (1). Sub-clinical AFib is implicated as a potential cause of embolic stroke of undetermined source (ESUS), and the current course of clinical care following ESUS is to look for evidence of AFib via an external monitor, an implanted loop recorder, or other forms of wearable monitoring devices. If AFib is diagnosed, treatment with oral anticoagulants is started to mitigate the possibility of recurrent stroke (2). Clinical studies have shown that AFib has been detected in only 30% of patients with long-term rhythm monitoring (3). This creates a frustrating problem for clinicians: in the wake of ESUS events, it is impossible to know which individuals should be treated as high-risk for AFib and therefore monitored accordingly.

Recent evidence from clinical studies suggests that the left atrial fibrosis burden measured by late gadolinium enhanced (LGE)-MRI is as high in ESUS patients as in AFib patients without stroke (4). This finding supports the hypothesis that atrial fibrosis is an element of the causal pathway for stroke, through an atrial cardiopathy, and independent of AFib. The absence of AFib despite the presence of a fibrotic substrate is intriguing and one potential explanation is that ESUS patients have pro-arrhythmic fibrotic substrate but lack the triggers needed to initiate arrhythmia. Another potential explanation is that the fibrosis present in ESUS patients is not pro-arrhythmic. Patient-derived computational modeling of atrial arrhythmias is uniquely poised to test these hypotheses. Previously, personalized atrial models have been used to assess arrhythmogenic propensity of fibrotic substrate and predict AFib ablation targets (5, 6). Applying the same approach, we can determine if, in the presence of appropriate triggers, fibrotic remodeling in ESUS patients has the fundamental capacity to harbor reentrant arrhythmic activity.

Thus, we present a large-scale computational study to ascertain whether the fibrotic substrate with the potential to perpetuate AFib-sustaining reentrant drivers (RDs) exists in ESUS patients. Our hypothesis is that a pre-clinical AFib substrate, attributed to a pattern of fibrotic atrial remodeling that is conducive to RD perpetuation, exists in ESUS patients. By conducting simulations in models derived from LGE-MRI, we can begin to understand potential pro-arrhythmic properties of atrial fibrosis in ESUS

patients. The study thus provides insights on the role of atrial fibrosis as a pathophysiological nexus between AFib and stroke.

Results

Patient Characteristics

Ninety patient-derived models were included in our analysis: 45 post-stroke ESUS and 45 pre-ablation AFib patients. Demographic information about both patient groups is provided in Table 1. There was a significant difference in LA surface area; however, the trend towards higher body mass index (BMI) in AFib patients and the lack of difference in LA volume index between the two groups suggests the latter trend (i.e., higher surface area in AFib) would be lessened if the values were normalized to body surface area. LA fibrosis burden was not significantly different between ESUS (13.6 ± 6.2%) and AFib patients (14.2 ± 4.5%) (P=0.91), consistent with previous findings (4).

	ESUS (N=45)	**AFib (N=45)**	**P value**
Age, y	60±16	62±12	0.504
Female, %	44.0%	32.8%	0.275
BMI, kg/m^2	27.6±4.3	29.5±5.9	0.08
CHA_2DVASc score	2.0	1.9	0.345
CHF, n	14.3%	18.4%	0.599
Hypertension, n	68.5%	61.2%	0.468
Diabetes mellitus, n	20.4%	12.2%	0.292
CAD, n	18.4%	18.4%	1.000
Smoking, n	32%	28%	0.679
LA fibrosis, %	13.6±6.2%	14.2±4.5%	0.91
LA surface area, cm^2	109±26	134±40	0.0007
LA volume index, mL/m^2	60±29	57±26	0.607

Table 1. *Patient characteristics in ESUS and AFib groups.*

Patient-derived model in silico AFib induction and fibrosis quantification

Personalized LA bilayer models were generated for all ESUS and AFib patients. Examples of physiological detail incorporated in models can be seen in Fig. 1, including patient-specific patterns of fibrotic remodeling, realistic atrial fiber orientations, and locations of electric pacing sites; further detail can be found in the Methods section. Rapid electric stimulation caused RD-sustained arrhythmia in 28 of 45 AFib models (62.2%) and 23 of 45 ESUS models (51.1%). Thus, the capability of the fibrotic substrate to sustain RDs was not significantly different between the two groups (P=0.39, Fig. 2A). ESUS and AFib patients were then sorted by amount of global LA fibrosis and arranged into quartiles. For five patients

(21.7%) in the first quartile (fibrosis<9.75%), six patients (29.0%) in the second quartile (fibrosis<12.6%), nineteen (79.2%) patients in the third quartile (fibrosis<17.45%), and twenty-one (95.5%) patients in the top quartile, simulations in the corresponding LA model revealed at least one pacing site for which stimulation produced an episode of RD-sustained arrhythmia (Fig. 2B).

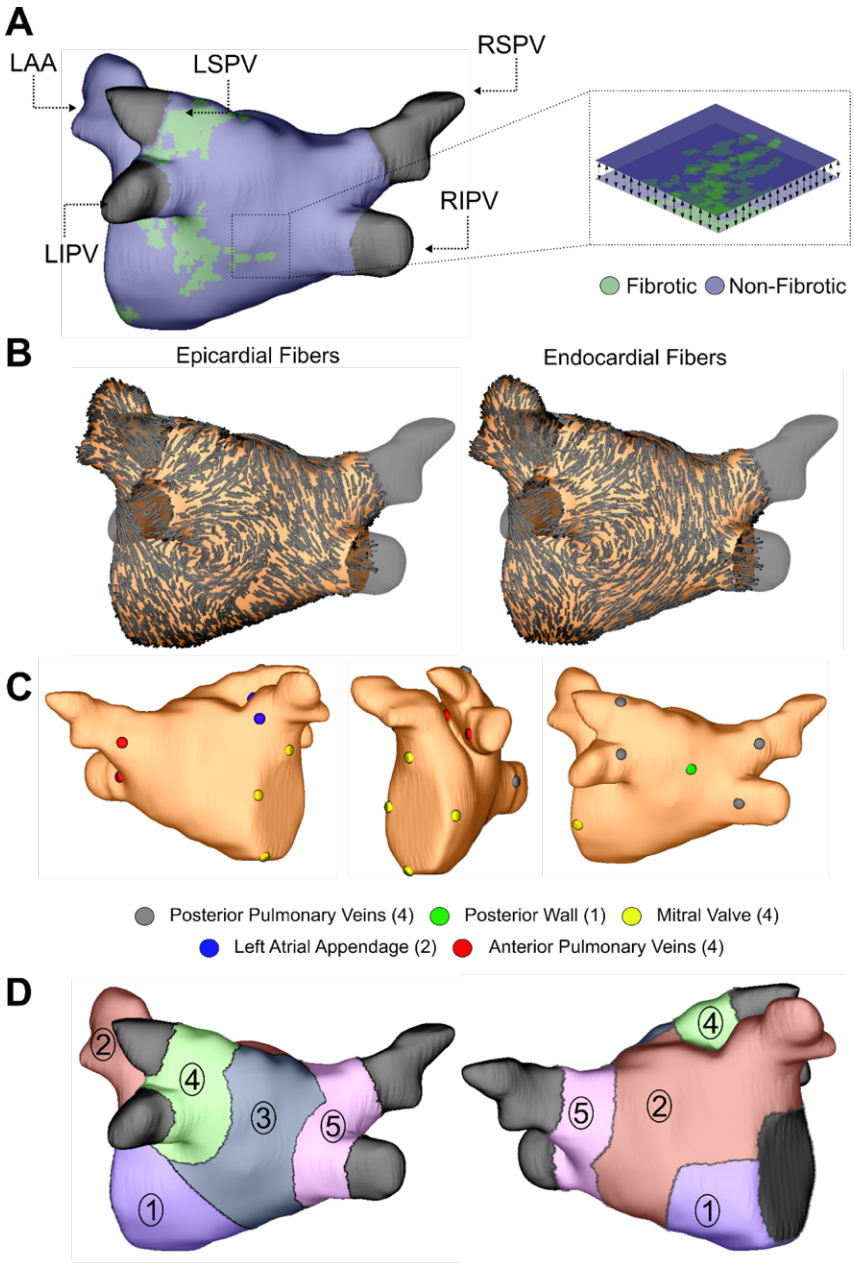

Figure 1 *Model generation (A) Reconstruction of LA geometry with anatomical features labelled (RIPV/RSPV/LIPV/LSPV, right/left inferior/superior pulmonary veins; LAA, LA appendage). The LA is modeled as a bilayer comprising nested endocardial and epicardial shells linked in both fibrotic and non-fibrotic regions by 1D linear elements. (B) LA fiber orientations for the endocardium and epicardium, mapped from human atlas geometry as described in Methods. (C) AFib trigger sites as pacing sites (posterior/anterior LIPV, LSPV, RSPV, RIPV, LAA base, mitral valve annulus and posterior wall). (D) Regions of the LA generated as described in methods: (1) atrial floor, (2) anterior wall and LAA, (3) posterior wall, (4) left PVs, (5) right PVs.*

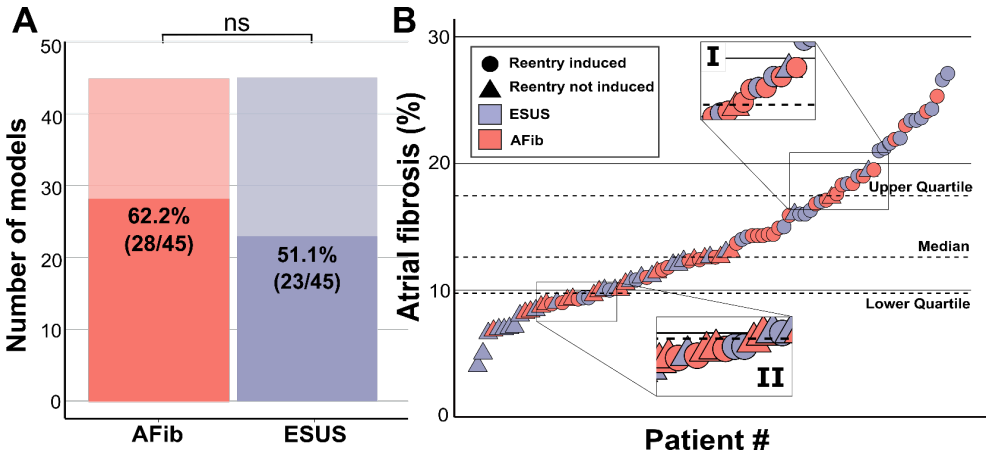

Figure 2 Summary of patient-derived model fibrosis with respect to RD inducibility. (A) Histogram of AFib (28/45) and ESUS (23/45) inducible patients. Inducibility was not significantly different by χ^2 test. (B) Patients with ESUS and AFib arranged by percentage of LA fibrosis. Dotted lines indicate the quartiles of fibrosis observed for all 90 patients. Circles are indicative of stable reentry observed in the model from at least one pacing site after *in silico* pacing protocol. Triangles indicate no RDs after pacing from all 15 pacing sites independently. Cases that lacked RDs despite high fibrosis (inset I) or were inducible despite low fibrosis (inset II) are highlighted.

To explore potential pro-arrhythmic substrate properties in ESUS and AFib, we analyzed fibrosis burden in the sub-groups of each cohort in which RD-sustained arrhythmias were inducible and non-inducible (Fig. 3A). Fibrosis burden was not significantly different between ESUS and AFib with (P=0.068, confidence interval; CI: [-0.2, 6.1], Fig. 3A) or without induced reentry (P=0.58, CI: [-2.4, 1.5], Fig. 3A). However, when fibrosis burdens for inducible and non-inducible models were aggregated across ESUS and AFib groups, a significant difference was evident (Fig. 3A; 16.8 ± 5.04% vs. 10.19 ± 3.14%; P<0.0001, CI: [4.4, 8.3]).

We also investigated potential differences in the number of unique RDs and the number of AFib triggers that induced reentry in each patient-derived model. In all 51 inducible models, the median number of unique RDs was 1.5 for AFib and 2 for ESUS models (range for both groups: 1-5). There was no significant difference in the number of unique reentrant morphologies per model between the two groups (Fig. 3B, P=0.79), CI: [$-1.6\text{x}10^{-5}$, 1]. The number of unique RDs was positively correlated with atrial fibrosis burden (Fig. 3C, R=0.69, P<0.0001). For all RD-inducible cases, the median number of stimulation sites from which rapid pacing led to RD formation was 2.5 for AFib and 3 for ESUS models (AFib range: 1-11; ESUS range: 1-7). No significant difference was found in the number of pacing sites that induced reentry per model between AFib and ESUS (Fig. 3D, P=0.98, CI [-1,1]). The number of RD inducing pacing sites was also significantly correlated with fibrosis burden (Fig. 3E, R=0.67, P<0.0001).

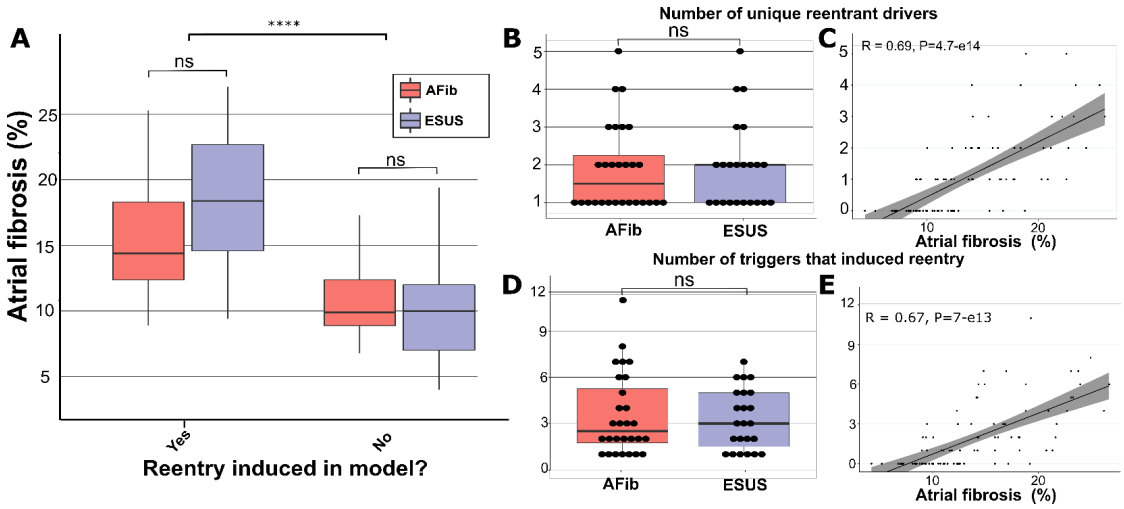

Figure 3 *Summary of RD characteristics between ESUS and AFib models. (A) Boxplot of fibrosis percentage in ESUS and AFib models where reentry was induced (ESUS: N=23, IQR=8.1; AFib: N=28, IQR=5.95) and where reentry was not induced (ESUS: N=22, IQR=4.98; AFib N=17, IQR=3.5). Across ESUS and AFib models, fibrosis burden for RD inducible and RD non-inducible models was significantly different (P<0.0001). (B) Boxplot of number of unique reentrant morphologies elicited by all 15 pacing sites (P=0.79). (C) Correlation plot of fibrosis vs number of RDs (R=0.69, P<0.0001) (D) Boxplot of the number of pacing sites which induced reentry (P=0.98) (E) Correlation plot of fibrosis vs number of pacing sites that induced reentry (R=0.67, P<0.0001).*

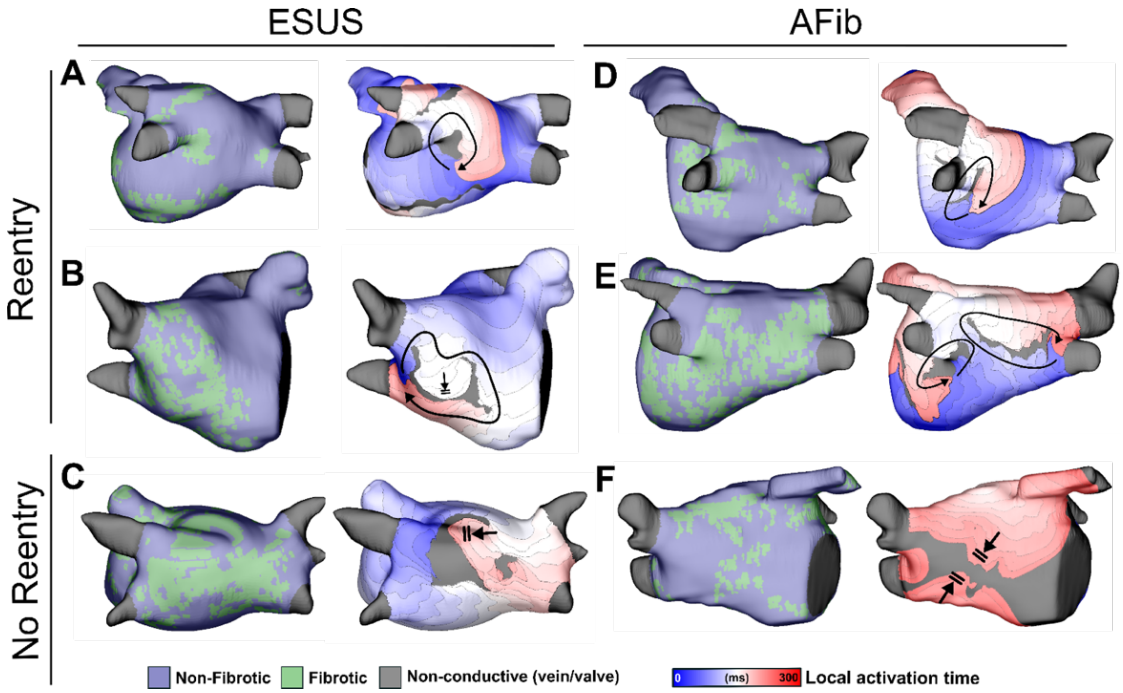

Figure 4. *Maps of fibrotic tissue distribution (left) and activation time (right) for ESUS and AFib models in which pacing succeeded (rows 1-2) or failed (row 3) to induce RD-driven arrhythmia. Black arrows indicate directions of wavefront propagation in RDs. Double lines indicate sites of conduction block. Black-shaded regions in activation maps indicate locations where activation did not occur during the analysis interval. (A) ESUS model with 10.8% fibrosis and reentry inferior to LIPV. (B) ESUS model with 10.0% fibrosis and reentry on anterior wall. (C) ESUS model with 19.4% fibrosis with wavefront termination through fibrosis on posterior wall. (D) AFib model with 9.0% fibrosis and reentry observed adjacent to RIPV on posterior wall. (E) AFib model with 24.1% fibrosis and reentry observed inferior to the LIPV and on posterior wall. (F) AFib model with 12.3% fibrosis with wavefront collision on posterior wall.*

Arrhythmia Dynamics

Analysis of simulated reentry episodes revealed no qualitative differences in arrhythmia dynamics between AFib and ESUS models. Figure 4 shows examples of RD-perpetuated *in silico* arrhythmia and instances where stimulation failed to induce reentry for both groups. Of note, this figure highlights two inducible low-fibrosis ESUS models (Fig. 4A: 10.8% fibrosis, RD near the LIPV; Fig. 4B: 10.0% fibrosis, RD in anterior wall) and a non-inducible high-fibrosis ESUS model (Fig. 4C: 19.4% fibrosis). In the latter case, dense fibrosis on the posterior wall resulted in conduction block as indicated. Similarly, Figs. 4D and 4E present examples of RD-driven arrhythmia in AFib models (9.0% and 24.1% fibrosis, respectively), and Fig. 4F shows an AFib model (12.3% fibrosis) in which reentry was not induced due to wavefront collision in the posterior wall region. Overall, this analysis shows that both ESUS and AFib models exhibited activation patterns consistent with previous definitions of RD-driven arrhythmia; examples of inducible low-fibrosis and non-inducible high-fibrosis models emphasize that fibrosis burden alone is an insufficient predictor for a potential arrhythmic substrate.

For 50/51 inducible models, AFib was driven by persistent singular RDs. In one AFib model we observed unique arrhythmia dynamics previously undocumented in atrial simulations, best described as dual RD feedback and characterized by interaction between two distinct wavefronts wherein one follows in the wake of another (Fig. 5 and Supplemental Video 1). Reentry appeared to occur as a result of a large central refractory region arising from wavefront collision adjacent to the RIPV on the septal face. This reentry morphology was stable for the duration of the simulation.

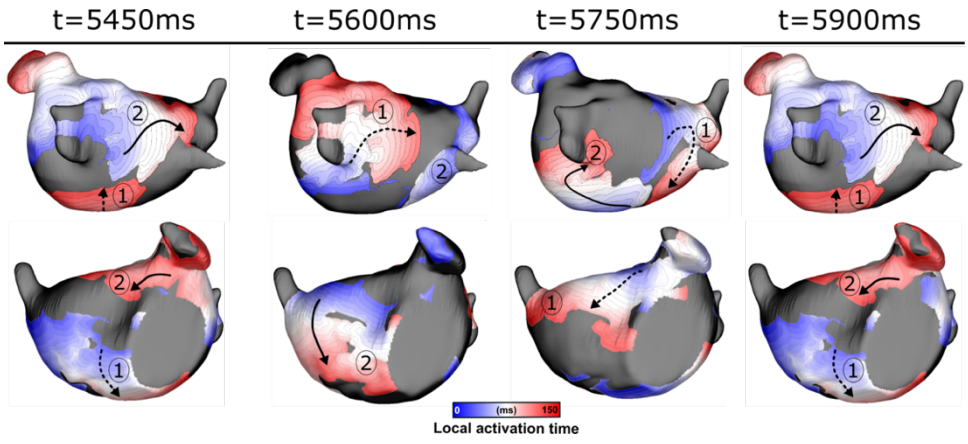

Figure 5. *Sequential activation maps showing one RD cycle of dual RD feedback viewed from posterior (top) and anterior (bottom) perspectives. Black-shaded region indicate locations where activation did not occur during the*

analysis interval. Activation maps at 5450ms progress to 5900ms in increments of 150ms. Two distinct wavefronts (labeled 1 and 2 in the panels above) exist in this form of reentry and "chase" after one another for duration of the simulation. See also Supplemental Video 1.

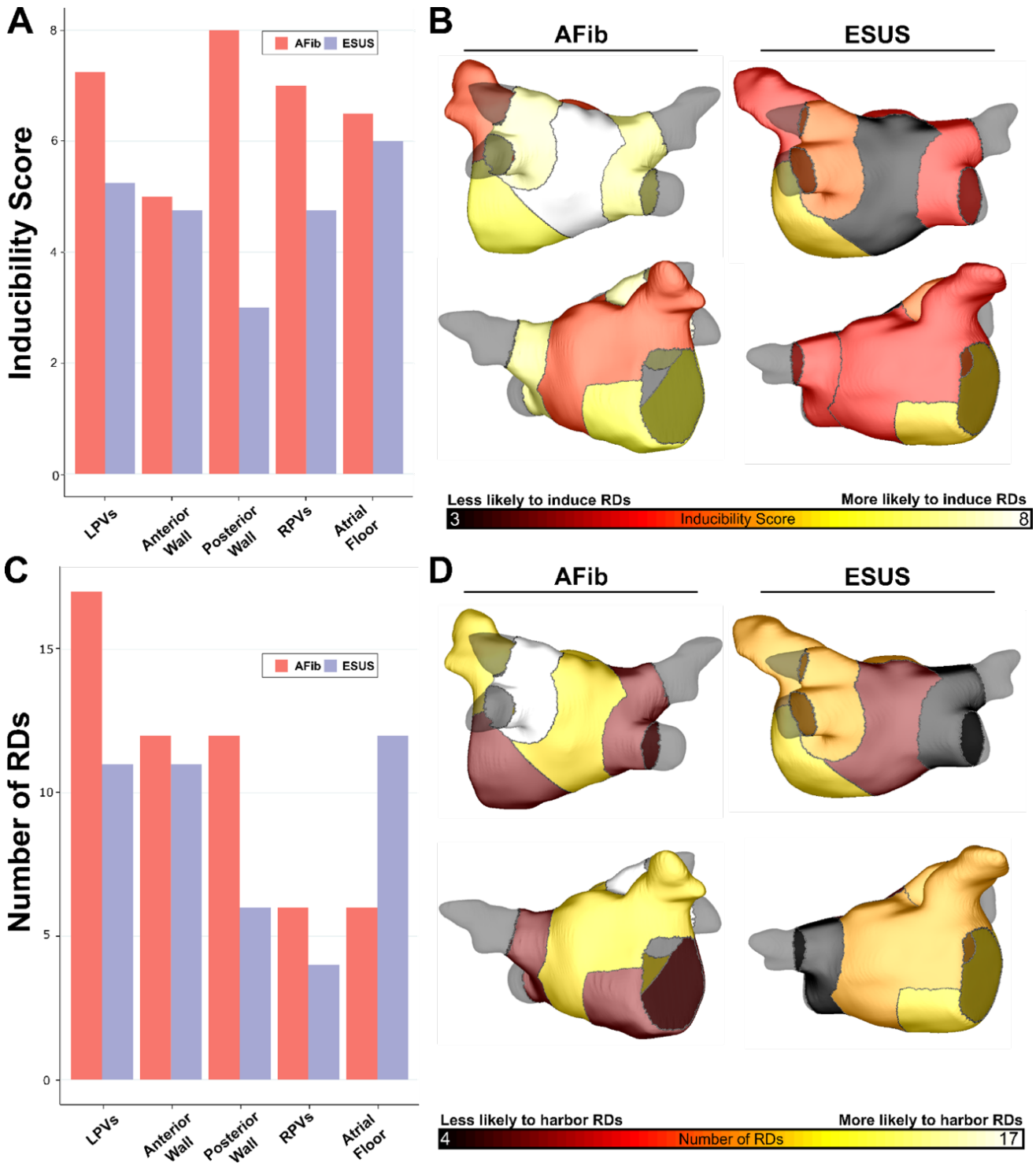

Figure 6. *Summary of IdS and RD localization characteristics. (A) Region-wise IdS for both ESUS and AFib LA models (B) Heat map of the regions in which triggers are most likely to induce arrhythmias depicted as representative ESUS and AFib models. (C) Histogram of RDs across all AFib and ESUS models binned by localization to specific LA regions. (D) Heat map of regions in which RDs are most likely to localize depicted as representative ESUS and AFib models.*

Properties of RD Localization

As described in Methods, each model was automatically subdivided into five anatomical regions (see schematic illustrations in Fig. 1D and Supplementary Fig. 1) and region-wise inducibility score analysis (IdS, as described in Methods) was used to gauge likelihood of RD induction in response to rapid electrical stimulation from different locations in the LA. While ESUS and AFib models had a statistically similar pattern of inducibility rates (P=0.73, by χ^2 test), stimulation from the posterior wall was ~3 times more likely to induce RDs in AFib models than ESUS models (Fig. 6A, IdS = 8 vs IdS = 3). In other words, with all other factors held equal, our simulations suggest that triggered activity in the posterior wall may be more likely to initiate reentrant arrhythmia in AFib patients compared to ESUS patients. The same IdS values plotted in Fig. 6A were mapped onto representative LA models to facilitate visual comparison of regional sensitivity to rapid pacing (Fig. 6B). Next, we considered the number of unique RD localization sites in each LA region across the different model groups (i.e., AFib vs. ESUS). The LPV region was most likely to harbor RDs in the AFib cohort (Fig. 6C, N=17). In the ESUS cohort, the atrial floor was the most likely region to contain an RD (N=12), whereas in the AFib cohort this was one of the least likely locations to harbor RDs (Fig. 6C, N=6). Of special note for the ESUS cohort, the atrial floor was both the most sensitive to rapid pacing in terms of RD initiation and the most likely area of RD localization (Fig. 6D). The association between the type of model (ESUS vs AFib) and RD localization was not significant (P=0.29, χ^2 test).

Discussion

This study used a novel computational modeling approach to shed new light on the role of the fibrotic atrial substrate in the potential for initiation and perpetuation of reentry in ESUS patients. In models reconstructed from 45 post-stroke ESUS and 45 pre-ablation AFib patients, we showed that the AFib and ESUS groups did not differ significantly in: (i) the propensity of the fibrotic substrate to sustain RDs in response to simulated burst pacing; (ii) the LA fibrotic burden of RD-inducible models or RD-free models; and (iii) the reentrant driver localization or the region-wise inducibility. This is the first study to use computational modeling and simulation to assess potential pro-arrhythmic capacity of LA fibrosis in ESUS patients. Moreover, to the best of our knowledge, this is the largest cohort ever studied via

computational analysis of atrial electrophysiology in models derived from LGE-MRI, exceeding the number of patients (N=50) in the former largest study (7) by a factor of ~1.8.

Inducibility of reentry and fibrosis quantification in patient-derived atrial models

Experimental findings have shown that atrial fibrosis results in changes that promote reentry (8, 9), but the exact mechanism of this connection is not fully understood. Previous modeling studies have linked RD localization to specific spatial patterns of fibrotic remodeling in AFib (5, 10). Recent clinical findings indicate that atrial fibrosis burden does not differ significantly between AFib and ESUS patients, and yet (by definition) ESUS patients do not demonstrate AFib at the time of stroke or during ambulatory monitoring (4). Given the findings summarized above, a potential explanation is that, notwithstanding the fact that ESUS patients have substantial fibrosis, the particular *spatial distribution* of fibrotic remodeling in their atria is not conducive to arrhythmia perpetuation. Our findings suggest that this is likely not the case. From the standpoint of computational models derived from patient LGE-MRI scans, fibrotic substrate in individuals with ESUS is indistinguishable from that in patients with AFib in terms of the fundamental capacity to sustain RDs. Reentrant arrhythmias were induced in 28/45 AFib models and 23/45 ESUS models (Fig. 2A). Across the combined set of 51 inducible models from both cohorts, we found that high fibrosis models were more likely to exhibit RDs irrespective of whether they corresponded to ESUS or AFib patients. This correlation has been characterized in prior AFib modeling studies (5, 6) and is consistent with established clinical thinking regarding the relationship between fibrosis and AFib outcomes (11). Notably, we did observe several cases in which models defied inducibility expectations based on fibrosis alone. Such models exhibited RDs despite low fibrosis or were non-inducible despite high fibrosis. This observation confirms that, as observed previously in analogous AFib modeling studies (5, 6), assessment of raw fibrosis burden LGE-MRI scans alone is insufficient to fully characterize arrhythmogenic capacity of potentially pro-arrhythmic substrate in ESUS.

Consistent with the goal of this research to understand the contribution of fibrotic substrate to potential RD formation in ESUS, we purposefully excluded arrhythmias perpetuated by other mechanisms from our study design (e.g., self-sustaining activity driven solely by focal sources). Potential contributions from the right atrium (RA) were also excluded, since only the LA was segmented from LGE-

MRI as part of the clinical workflow. Either of these factors may explain the absence of simulated arrhythmia in 17 of 45 AFib models, many of which had very little LA fibrosis (i.e., AFib in these individuals might have been predominantly focal in nature or sustained by RDs in the RA). This rate of inducibility is consistent with previous studies (e.g.,13 out of 20 in computational models reconstructed from LGE-MRI scans of persistent AFib patients) (5), supporting the notion that LA fibrosis is associated with increased arrhythmia inducibility but fails to tell the whole story. Importantly, neither of these model constraints repudiates the central finding of our study, which suggests there is no difference between ESUS and AFib patients in terms of the fundamental capacity of the fibrotic substrate to potentially harbor RDs.

Reentrant driver localization dynamics and morphology in patient-derived atrial models

As discussed above, our qualitative findings suggest that ESUS patients' fibrotic substrate is no different than that of AFib patients in terms the capacity to sustain RDs per se. We performed additional analysis to assess whether specific consequences of fibrotic remodeling influenced any characteristics of RD inducibility in different ways for simulations in models corresponding to ESUS vs. AFib patients. First, we found that there was no significant difference in global fibrosis burden between the 28 inducible AFib models and the 23 inducible ESUS models (Fig. 3A). This finding suggests that intrinsic pro-arrhythmic characteristics of the fibrotic substrate in ESUS and AFib patients are indistinguishable, which is a key finding of this study. Given this result, one potential alternative explanation for the lack of arrhythmia in ESUS patients is a lack of suitable triggers, despite an abundance of fibrotic substrate on par with that observed in AFib. The plausibility of this explanation is strengthened by the fact that the pacing sites from which episodes of reentry were induced in our study were based on common AFib trigger sites as identified in a recent clinical study (12); this is in contrast to previous modeling studies, which simulated triggered activity from evenly-distributed atrial sites (6). However,, the premise of this aspect of our work was not to assess an absence of triggers, but instead ask the following: if the atria of these ESUS patients were subjected to the same type of triggered activity known to occur in typical AFib patients, is it possible the result be would sustained arrhythmia? In more than half of the cohort (23/45), our analysis suggests that the answer is yes.

A potential implication of our study is that in AFib patients, pathological changes in geometry, specifically increased LA surface area (134±40 cm^2 for AFib vs. 109±26 cm^2 for ESUS; P=0.0007; see Table 1), and fibrotic remodeling may interact synergistically to promote RD formation. Other measurements (BMI, LA volume index) suggest this difference might be abolished by normalizing these values to body surface area. However, we opted to present absolute LA surface area values since a relevant metric for arrhythmia perpetuation is effective heart size (i.e., ratio between absolute heart size and cardiac wavelength) (13). In effect, larger effective heart size implies that reentrant wavefronts have more "elbow room" to establish and anchor themselves, increasing the likelihood of sustained RD occurrence. Thus, this may explain the trend towards higher burden of fibrosis in inducible ESUS models vs. inducible AFib models (Fig. 3A, P=0.068). Since ESUS patients lack the anatomical LA remodeling observed in AFib patients, a higher threshold of fibrotic tissue may be necessary in order for RD-driven arrhythmia to be even theoretically possible. More work is needed to concretely validate this finding.

Further analysis was performed to probe potential differences between ESUS and AFib patients that went beyond consideration of RD inducibility as a binary variable. Specifically, we found no significant difference (P=0.79) in the number of unique model-predicted RDs between ESUS and AFib (range for both groups: 1-5; Fig. 3B). Instead, the number of unique RDs was highly correlated (Fig. 3C, R=0.69, P<0.0001) with LA fibrosis burden, which is consistent with the concept that high fibrosis models are more likely to exhibit RDs. Secondly, analysis of the number of pacing sites that induced RDs revealed high variability (range: 0-11 out of 15), but again the ESUS and AFib groups were similar in this regard (Fig. 3D, P=0.98). This variable was also correlated to LA fibrosis burden (R=0.67, P<0.0001), suggesting greater fibrotic remodeling leads to susceptibility to pacing-induced reentry by triggered activity from a larger number of locations. This finding further substantiates our principal claim that no significant differences exist between the detected fibrotic substrate in ESUS and AFib, in that it holds true for the substrate's capacity to sustain reentry and its susceptibility to triggered activity. The general implication is that in the presence of simulated triggered activity, both of these characteristics are closely linked to global fibrosis burden.

RDs identified by non-invasive electrocardiographic imaging (ECGI) and *in silico* phase singularity identification have been shown to co-localize with fibrosis boundary zones identified by LGE-MRI (5, 14-16). RD localization dynamics in this study were consistent with these findings, as illustrated by representative LA fibrotic tissue distributions and corresponding RD activation patterns in Fig. 4. RD morphology in this study, for both AFib and ESUS models, largely corroborated previous findings – arrhythmia episodes were perpetuated by one RD at a time, with activity in the periphery including conduction block, transient reentry, and wavefront collision (5, 6). There was one noteworthy exception, which was the dual reciprocating RD interaction documented in Fig. 5, in which a region of conduction block formed dynamically in the myocardial region between the two circulating wavefronts. Similar excitation sequences have been documented previously in embryonic chick cardiac cells (17) and in patients with atypical flutter (18). It is unclear why we observed this behavior for the first time in this study despite the fact that over 100 episodes of RD-driven arrhythmia have been simulated in dozens of similarly constructed models (5, 6, 19). A potential explanation is the use of increased tissue conductivity in the present study, resulting in faster conduction velocity.

Insights from analysis of RD inducibility and localization by LA region

Our findings thus far demonstrate that the properties of simulated RDs are indistinguishable between ESUS and AFib. We then performed region-wise analysis to assess any systematic differences in the spatial distribution of pro-arrhythmic fibrosis that could render certain regions more susceptible to either triggered activity or RD-localization. Even when analyzing the atria by distinct regions, we found that the spatial properties of the fibrotic substrate between AFib and ESUS patients are not intrinsically different. ESUS and AFib models had no significant association to either reentrant driver localization or region-wise inducibility ($P=0.73$ and $P=0.29$, by χ^2 test). However, our region-wise analysis (Fig. 6) did yield several noteworthy findings that suggest subtle distinctions in the spatial distribution of pro-arrhythmic fibrosis may exist between the two groups. While non-PV LA triggers have been identified (posterior wall, appendage, mitral valve) (12), the PVs are considered the main source of focal activity responsible for initiating AFib episodes (20, 21). In light of this fact, it is notable that our modeling suggests triggered activity in the LPV and RPV regions is ~50% more likely to induce reentrant arrhythmia

in AFib vs. ESUS models (i.e., IdS ≈ 7.5 vs. 5). An even more striking differential exists for the posterior wall region, where the IdS score was ~3x higher in AFib compared to ESUS models. This observation suggests that even in the cases when common potential LA triggers, such as (i.e., PV or posterior wall ectopy) do occur in ESUS patients, they are less likely to engage the fibrotic substrate and initiate sustained reentry compared to the same activity in AFib patients. This possibility does not contradict our hypothesis that the lack of arrhythmia in ESUS is due to a dearth of triggers; rather, it is a complementary corollary that can be put to the test in future clinical and computational analysis.

While understanding of RD localization dynamics in AFib remains limited, evidence from ECGI mapping indicates that reentrant activity occurs most frequently in the PV and posterior wall regions (15, 20, 21). Our findings are consistent with these data, with those same three areas harboring a majority (~70%) of all observed RDs in models corresponding to AFib patients. In contrast, in the ESUS population the atrial floor was the RD localization hotspot. The importance of this finding is unclear as tendencies toward reentrant activity in particular LA areas has not been meaningfully correlated to clinical arrhythmia properties. However, it provides a path for future validation studies: if incident AFib in patients who previously presented with ESUS can be characterized by intracardiac mapping, the hypothesis that RDs localize preferentially to the atrial floor can be tested.

Finally, across both ESUS and AFib cohorts we observed that LA regions with the highest IdS generally corresponded to areas most likely to harbor RDs. The implication is that despite some interesting and noteworthy trends in region-wise substrate susceptibility between ESUS and AFib, the overarching conclusion of our analysis remains unchanged: we hypothesize that if the ESUS substrate were subjected to suitable triggered activity, it would be fully capable of sustaining RDs indistinguishable from those that perpetuate AFib.

Limitations

In this study, atrial tissue is modeled as a bilayer to drastically reduce computational load. Previous studies have used this modeling framework (14, 22) to represent human atria effectively, but the framework remains a simplification compared to volumetric 3D models. Moreover, clinical-grade MRI resolution limits our ability to detect fine details in anatomical structure and spatial distribution of

potentially arrhythmogenic substrate, for instance slow-conducting tracks of fibrotic atrial tissue that could underlie microreentrant circuits (23). While these models are patient-specific in terms of LA anatomy and each individual's unique pattern of fibrotic remodeling, they do not incorporate inter-patient variability in CV and electrophysiological properties such as ion channel expression. Nevertheless, our previous analysis indicates that this representation of atrial architecture with generic "average AFib" electrophysiology is appropriate for use in patient-derived modeling (10, 24).

As in previous studies (25, 26), our models do not differentiate between cell- or tissue-scale properties of atrial electrophysiology between patients with paroxysmal and persistent forms of AFib. Likewise, our approach to characterizing potential arrhythmia propensity in ESUS patients assumes cell- and tissue-scale remodeling based on experimental and clinical data from the AFib milieu. Although this is relevant as a limitation and must be considered when interpreting our results, this aspect of our approach is also one of the major advantages of the modeling and simulation methodology. Specifically, it allows us to assess whether there are any relevant differences in the spatial pattern of fibrotic remodeling between ESUS and AFib patients in the absence of other potentially confounding variables.

Finally, the mechanism of stroke in ESUS patients may be independent of the presence of AFib and atrial fibrosis through decreased atrial function might be a contributor to thrombus formation in the absence of AFib. Currently, secondary stroke prophylaxis is dependent on detecting AFib and predicting, through computational modeling, which atria are more prone to manifest AFib may be of clinical value. Another future research direction that could prove highly fruitful in the near future would be to create multi-scale, multi-physics image-based models of the fibrotic atria to assess each individual's risk of clot formation in a patient-specific manner.

Conclusions

Simulations suggest that the pro-arrhythmic properties of fibrotic substrate in ESUS and AFib patients are indistinguishable. Our results show that fibrotic remodeling in ESUS patients has the theoretical capacity to sustain reentry when subjected to common AFib triggers. Thus, we conclude that fibrotic substrate conducive to perpetuating reentry may exist in up to half of ESUS patients. As individuals studied in this cohort present with incident AFib over the next few years, we will be able to put

this hypothesis to the test. Our findings also support the notion that the lack of AFib in this population may be attributable to a lack of suitable arrhythmic triggers, but further research is needed to fully justify this claim. While the existence of pre-clinical substrate is correlated with a higher global proportion of fibrotic tissue, many ESUS cases defied these expectations, suggesting that fibrosis burden alone is insufficient for predicting pre-clinical AFib substrate. This conclusion justifies the use of computational simulations to probe beyond the fibrosis as imaged. Overall, these results provide novel insights into the role of atrial fibrotic remodeling as a critical nexus between the otherwise distinct manifestations of AFib and ESUS.

Materials and Methods

Patient Population

Patients were recruited to undergo cardiac LGE-MRI from the University of Washington (Seattle, WA) and Klinikum Coburg (Coburg, Germany) between July 2016 and June 2019. This study was approved by the Institutional Review Board (IRB) of the University of Washington (UW) and the Ethikkommission der Bayerischen Ländesärztekammer München, Bayern, Deutschland; all participants provided written informed consent. Patients with ESUS met published diagnostic criteria (27). Patients with paroxysmal (27/45, 60%) or persistent AFib and without stroke were recruited from the UW Cardiac Arrhythmia Data Repository, an IRB-approved database for arrhythmia patients. Exclusion criteria for AFib patients included those who had undergone LA catheter ablation before MRI and those with only atrial flutter. Patients with cardiac implantable electronic devices, severe claustrophobia, renal dysfunction, and other contraindications to MRI or gadolinium-based contrast were excluded.

MRI acquisition

Cardiac LGE-MRI was obtained on all participants to quantify the extent of LA fibrosis using previously described protocols (11). Scans were performed on Philips Ingenia and Siemens Avanto clinical scanners, 15 to 25 minutes after contrast injection, using a 3-dimensional inversion-recovery, respiration-navigated, ECG-gated, gradient echo pulse sequence. Acquisition parameters included transverse imaging volume with a voxel size of 1.25 x 1.25 x 2.5 mm (reconstructed to 0.625 x 0.625 x

1.25 mm). Scan time was 5 to 10 minutes dependent on respiration and heart rate. Fat saturation sequences were used to suppress signal from fatty tissue.

Reconstruction of 3D patient-derived atrial models from LGE-MRI

Geometric models were reconstructed from LGE-MRI and the relative extent of fibrosis in the LA was quantified via an adaptive histogram thresholding algorithm (28). Clinical-grade meshes (i.e., coarse discretization) produced by Merisight Inc. (Salt Lake City, UT) were resampled with a target resolution of 200 μm using an automated process based on gmsh (29). Each LA model was represented as a bilayer comprising of nested endocardial and epicardial shells, linked at every point by linear connections (σ = 0.8 S m^{-1}) (Fig. 1A). In each patient-derived model, realistic myocardial fiber orientations were mapped from an atlas geometry (22) using the universal atrial coordinates (UAC) approach. Briefly, this process assigned epicardial and endocardial fibers from a previously published bilayer model to the target atrial geometry (Fig. 1B) (30, 31). In all finite element LA meshes, the average element edge length was ~188 μm and the number of nodes ranged from ~600,000 to ~1.4 million, depending on LA size. This mesh resolution is consistent with previously established benchmarks for minimizing numerical error due to spatial discretization in simulations of cardiac wavefront propagation (32).

Modeling of atrial electrophysiology in fibrotic and non-fibrotic regions

Our methodology for computational modeling at the cell and tissue scale of the fibrotic and non-fibrotic atrial electrophysiology can be found in previously published papers (5, 15, 19). Briefly, in non-fibrotic regions, a human atrial action potential model (33) was used to represent membrane kinetics, including parameter modifications to fit clinical monophasic action potential recordings from AFib patients (I_{Kur}, I_{to}, I_{CaL} decreased by 50%, 50%, 70%, respectively) (5, 34). At the tissue scale, non-fibrotic atrial tissue, conductivity tensor values (longitudinal: $\sigma_L = 0.409\ S\ m^{-1}$; transverse: $\sigma_T = 0.08195\ S\ m^{-1}$) were calibrated to obtain effective conduction velocity (CV) values of 71.49 $cm\ s^{-1}$ and 37.14 $cm\ s^{-1}$ (longitudinal and transverse). These conductivities were chosen to match, CV values measured in AFib patients (61±6 cm/s) (35). In fibrotic regions, modifications to the AFib-like action potential model (ICaL, I_{Na}, and I_{K1} decreased by 50%, 40%, 50%, respectively) were implemented as in prior studies (5, 36), resulting in a 15.4% increase in action potential duration and a 49.6% decrease in upstroke velocity.

These changes represented the effect of elevated transforming growth factor-β1, a key component of the fibrogenic signaling pathway. As in previous studies (5, 15, 19), tissue-scale effects of interstitial fibrosis and gap junction remodeling were represented by reducing overall conductivity and exaggerating the anisotropy ratio (σ_L:σ_T) from 5:1 to 8:1 ($\sigma_L = 0.17708$ S m^{-1}; $\sigma_T = 0.022135$ S m^{-1}).

Simulation of electrical activity and numerical aspects

Electrical propagation in LA models was simulated by solving the monodomain equation using the finite element method. This system was coupled with ordinary differential and algebraic equations representing myocyte membrane dynamics at each node in the mesh, as described in the prior section. All simulations were executed on the Hyak supercomputer system at the University of Washington using the CARP software package (37, 38). A free version of CARP is available for academic use (see: https://openCarp.org). The compute time required to complete each unique simulation ranged from 1-10 hours. The total CPU time for all simulations conducted in all models was 13.4 years.

Induction and analysis of reentrant atrial arrhythmias

Simulations were performed to assess the pro-arrhythmic propensity of the fibrotic substrate in each patient-derived model. Arrhythmia induction via rapid pacing was attempted from 15 pacing sites derived from AFib trigger sites (Fig. 1C, see caption for detailed anatomical site descriptions) (12). Clinically relevant AFib trigger sites were chosen over a random pacing schematic to specifically capture RDs that arise from locations demonstrated to induce AFib. Similar to previous publications, a clinically relevant pacing sequence of 12 electrical stimuli was delivered at each of the 15 locations (5, 36). Individual cell-scale ionic models were paced to steady-state at a rate basic cycle length of 500 ms. The electrical stimulus consisted of two initial pulses with a coupling interval of 300ms, followed by pulses ramping down to 200ms in 20ms intervals. After the delivery of the final stimulus, simulations were monitored for self-sustaining electrical wavefront propagation. For all cases in which activity persisted for at least 5,000ms post-pacing, we applied further analysis to determine whether the cause was an induced RD or macroscopic re-entry (i.e. continuous repetitive, self-sustaining activation propagating around a non-conductive obstacle such as the mitral valve or pulmonary vein(s)), which we consider flutter-like reentry. Instances of macroscopic re-entry were excluded from further analysis.

For each AFib-inducible simulation, we documented whether each pacing site induced reentry and analyzed patterns of RD localization. Unique RD morphologies in each patient-derived model were classified as being located in one of five anatomical regions (Fig. 1D). These regions were delineated automatically in a two-step process summarized in Supplemental Fig. 1. First, the LA was subdivided into three broad anatomical areas (region 1: LA floor, 2: posterior wall; 3: anterior wall including LAA) using standardized cutoff values in the UAC space (30). Second, the left and right PV areas (regions 4 and 5, respectively) were established using a region-growing approach such that each accounted for 15% of the total LA surface area. We then defined region-wise inducibility scores (IdS) across all models in a particular group (ESUS or AFib) as the proportion of pacing sites within a given region from which rapid pacing resulted in initiation of an RD. For example, since the LPV region contains four pacing sites (anterior/posterior LSPV/LIPV), the corresponding ESUS IdS value would be derived by summing the number of instances in which pacing from those locations induced RD across inducible ESUS models then dividing by four. This ensured our ability to assess spatial heterogeneity of sensitivity to triggered activity in a manner that was unbiased to the relative abundance of pacing sites in some LA regions.

Statistical Analysis

LA models for ESUS and AFib patients were divided into quartiles based on the extent of fibrotic remodeling as measured by LGE-MRI. Continuous variables were compared pairwise between groups using Wilcoxon rank-sum tests and were reported as mean ± standard deviation. Confidence intervals were calculated as the interval for the true difference in mean with 95% certainty. Categorical variables were compared using a χ^2 test. After classifying unique RDs and number of pacing sites that induced reentry, correlation with fibrosis was assessed with logistic regression. Statistical significance was established at two-tailed $P \leq 0.05$. All statistical analysis was performed using R (39).

Author Contributions: SFB, NA, and PMB designed the study; SFB, GDS, and PMB built models, conducted simulations, and analyzed computational results; CHR and SAN provided their implementation of the UAC methodology and expertise on how to use it in model reconstruction; CM, PK, MM, and NA were responsible for acquisition of cardiac LGE-MRI data; SS, ZB, CM, PK, MM, DT, WTL, and NA analyzed clinical data; SFB, NA, and PMB wrote the manuscript with feedback from all co-authors.

Acknowledgments: SFB is supported by a fellowship from the ARCS foundation. CHR is supported by a Medical Research Council Skills Development Fellowship (MR/S015086/1). SAN is supported by NIH R01-HL152256, ERC PREDICT-HF (864055), BHF (RG/20/4/34803), EPSRC (EP/P01268X/1), and the Wellcome Trust (203148/Z/16/Z). DT and WTL are co-PIs for the ARCADIA trial (NIH 5-U01-NS095869), which receives in-kind study drug from the BMS-Pfizer Alliance and ancillary funding from Roche Diagnostics. NA is supported by John Locke Charitable Trust.

References

1. Andrade J, Khairy P, Dobrev D, Nattel S. The clinical profile and pathophysiology of atrial fibrillation: relationships among clinical features, epidemiology, and mechanisms. Circ Res. 2014;114(9):1453-68.
2. Israel C, Kitsiou A, Kalyani M, Deelawar S, Ejangue LE, Rogalewski A, et al. Detection of atrial fibrillation in patients with embolic stroke of undetermined source by prolonged monitoring with implantable loop recorders. Thromb Haemost. 2017;117(10):1962-9.
3. Brachmann J, Morillo CA, Sanna T, Di Lazzaro V, Diener HC, Bernstein RA, et al. Uncovering Atrial Fibrillation Beyond Short-Term Monitoring in Cryptogenic Stroke Patients: Three-Year Results From the Cryptogenic Stroke and Underlying Atrial Fibrillation Trial. Circ Arrhythm Electrophysiol. 2016;9(1):e003333.
4. Tandon K, Tirschwell D, Longstreth WT, Jr., Smith B, Akoum N. Embolic stroke of undetermined source correlates to atrial fibrosis without atrial fibrillation. Neurology. 2019;93(4):e381-e7.
5. Zahid S, Cochet H, Boyle PM, Schwarz EL, Whyte KN, Vigmond EJ, et al. Patient-derived models link re-entrant driver localization in atrial fibrillation to fibrosis spatial pattern. Cardiovasc Res. 2016;110(3):443-54.
6. Boyle PM, Zghaib T, Zahid S, Ali RL, Deng D, Franceschi WH, et al. Computationally guided personalized targeted ablation of persistent atrial fibrillation. Nat Biomed Eng. 2019;3(11):870-9.
7. Roney CH, Beach ML, Mehta A, Sim I, Corrado C, Bendikas R, et al. In silico comparison of left atrial ablation techniques that target the anatomical, structural and electrical substrates of atrial fibrillation. Front Physiol. 2020.
8. Xia Y, Hertervig E, Kongstad O, Ljungstrom E, Platonov P, Holm M, et al. Deterioration of interatrial conduction in patients with paroxysmal atrial fibrillation: electroanatomic mapping of the right atrium and coronary sinus. Heart Rhythm. 2004;1(5):548-53.
9. Litchenberg WH, Norman LW, Holwell AK, Martin KL, Hewett KW, Gourdie RG. The rate and anisotropy of impulse propagation in the postnatal terminal crest are correlated with remodeling of Cx43 gap junction pattern. Cardiovasc Res. 2000;45(2):379-87.
10. Hakim JB, Murphy MJ, Trayanova NA, Boyle PM. Arrhythmia dynamics in computational models of the atria following virtual ablation of re-entrant drivers. Europace. 2018;20(suppl_3):iii45-iii54.
11. Marrouche NF, Wilber D, Hindricks G, Jais P, Akoum N, Marchlinski F, et al. Association of atrial tissue fibrosis identified by delayed enhancement MRI and atrial fibrillation catheter ablation: the DECAAF study. JAMA. 2014;311(5):498-506.
12. Santangeli P, Marchlinski FE. Techniques for the provocation, localization, and ablation of non-pulmonary vein triggers for atrial fibrillation. Heart Rhythm. 2017;14(7):1087-96.

13. Panfilov AV. Is heart size a factor in ventricular fibrillation? Or how close are rabbit and human hearts? Heart Rhythm. 2006;3(7):862-4.
14. Roney CH, Bayer JD, Zahid S, Meo M, Boyle PM, Trayanova NA, et al. Modelling methodology of atrial fibrosis affects rotor dynamics and electrograms. Europace. 2016;18(suppl 4):iv146-iv55.
15. Boyle PM, Hakim JB, Zahid S, Franceschi WH, Murphy MJ, Vigmond EJ, et al. Comparing Reentrant Drivers Predicted by Image-Based Computational Modeling and Mapped by Electrocardiographic Imaging in Persistent Atrial Fibrillation. Front Physiol. 2018;9:414.
16. Cochet H, Dubois R, Yamashita S, Al Jefairi N, Berte B, Sellal JM, et al. Relationship Between Fibrosis Detected on Late Gadolinium-Enhanced Cardiac Magnetic Resonance and Re-Entrant Activity Assessed With Electrocardiographic Imaging in Human Persistent Atrial Fibrillation. JACC Clin Electrophysiol. 2018;4(1):17-29.
17. Campanari L, You MJ, Langfield P, Glass L, Shrier A. Varieties of reentrant dynamics. Chaos. 2017;27(4):041101.
18. Cheng J, Scheinman MM. Acceleration of typical atrial flutter due to double-wave reentry induced by programmed electrical stimulation. Circulation. 1998;97(16):1589-96.
19. Boyle PM, Hakim JB, Zahid S, Franceschi WH, Murphy MJ, Prakosa A, et al. The Fibrotic Substrate in Persistent Atrial Fibrillation Patients: Comparison Between Predictions From Computational Modeling and Measurements From Focal Impulse and Rotor Mapping. Front Physiol. 2018;9:1151.
20. Haissaguerre M, Hocini M, Denis A, Shah AJ, Komatsu Y, Yamashita S, et al. Driver domains in persistent atrial fibrillation. Circulation. 2014;130(7):530-8.
21. Tanaka K, Zlochiver S, Vikstrom KL, Yamazaki M, Moreno J, Klos M, et al. Spatial distribution of fibrosis governs fibrillation wave dynamics in the posterior left atrium during heart failure. Circ Res. 2007;101(8):839-47.
22. Labarthe S, Bayer J, Coudiere Y, Henry J, Cochet H, Jais P, et al. A bilayer model of human atria: mathematical background, construction, and assessment. Europace. 2014;16 Suppl 4:iv21-iv9.
23. Hansen BJ, Zhao J, Li N, Zolotarev A, Zakharkin S, Wang Y, et al. Human Atrial Fibrillation Drivers Resolved With Integrated Functional and Structural Imaging to Benefit Clinical Mapping. JACC Clin Electrophysiol. 2018;4(12):1501-15.
24. Deng D, Murphy MJ, Hakim JB, Franceschi WH, Zahid S, Pashakhanloo F, et al. Sensitivity of reentrant driver localization to electrophysiological parameter variability in image-based computational models of persistent atrial fibrillation sustained by a fibrotic substrate. Chaos. 2017;27(9):093932.
25. Ali RL, Hakim JB, Boyle PM, Zahid S, Sivasambu B, Marine JE, et al. Arrhythmogenic propensity of the fibrotic substrate after atrial fibrillation ablation: a longitudinal study using magnetic resonance imaging-based atrial models. Cardiovasc Res. 2019;115(12):1757-65.
26. Shade JK, Ali RL, Basile D, Popescu D, Akhtar T, Marine JE, et al. Preprocedure Application of Machine Learning and Mechanistic Simulations Predicts Likelihood of Paroxysmal Atrial Fibrillation Recurrence Following Pulmonary Vein Isolation. Circ Arrhythm Electrophysiol. 2020;13(7):e008213.
27. Hart RG, Catanese L, Perera KS, Ntaios G, Connolly SJ. Embolic Stroke of Undetermined Source: A Systematic Review and Clinical Update. Stroke. 2017;48(4):867-72.

28. Jadidi AS, Cochet H, Shah AJ, Kim SJ, Duncan E, Miyazaki S, et al. Inverse relationship between fractionated electrograms and atrial fibrosis in persistent atrial fibrillation: combined magnetic resonance imaging and high-density mapping. J Am Coll Cardiol. 2013;62(9):802-12.

29. Geuzaine C, Remacle J-F. Gmsh: A 3-D finite element mesh generator with built-in pre- and post-processing facilities. International Journal for Numerical Methods in Engineering. 2009;79(11):1309-31.

30. Roney CH, Pashaei A, Meo M, Dubois R, Boyle PM, Trayanova NA, et al. Universal atrial coordinates applied to visualisation, registration and construction of patient specific meshes. Med Image Anal. 2019;55:65-75.

31. Roney CH, Bendikas R, Pashakhanloo F, Corrado C, Vigmond EJ, McVeigh ER, et al. Constructing a Human Atrial Fibre Atlas. Ann Biomed Eng. 2020.

32. Niederer SA, Kerfoot E, Benson AP, Bernabeu MO, Bernus O, Bradley C, et al. Verification of cardiac tissue electrophysiology simulators using an N-version benchmark. Philos Trans A Math Phys Eng Sci. 2011;369(1954):4331-51.

33. Courtemanche M, Ramirez RJ, Nattel S. Ionic mechanisms underlying human atrial action potential properties: insights from a mathematical model. Am J Physiol. 1998;275(1):H301-21.

34. Krummen DE, Bayer JD, Ho J, Ho G, Smetak MR, Clopton P, et al. Mechanisms of human atrial fibrillation initiation: clinical and computational studies of repolarization restitution and activation latency. Circ Arrhythm Electrophysiol. 2012;5(6):1149-59.

35. Konings KT, Kirchhof CJ, Smeets JR, Wellens HJ, Penn OC, Allessie MA. High-density mapping of electrically induced atrial fibrillation in humans. Circulation. 1994;89(4):1665-80.

36. Zahid S, Whyte KN, Schwarz EL, Blake RC, 3rd, Boyle PM, Chrispin J, et al. Feasibility of using patient-specific models and the "minimum cut" algorithm to predict optimal ablation targets for left atrial flutter. Heart Rhythm. 2016;13(8):1687-98.

37. Vigmond EJ, Hughes M, Plank G, Leon LJ. Computational tools for modeling electrical activity in cardiac tissue. J Electrocardiol. 2003;36 Suppl:69-74.

38. Vigmond EJ, Weber dos Santos R, Prassl AJ, Deo M, Plank G. Solvers for the cardiac bidomain equations. Prog Biophys Mol Biol. 2008;96(1-3):3-18.

39. R Development Core Team. R: A language and environment for statistical computing. Vienna, Austria: R Fonudation for Statistical Computing; 2019.

Supplemental Information

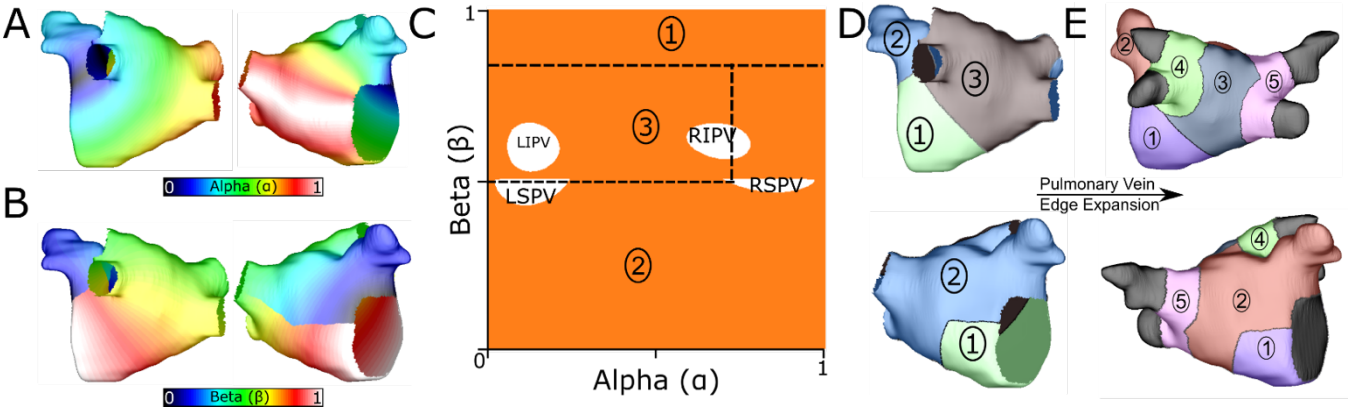

Supplemental Figure 1. LA subdivision scheme. (A) Alpha coordinate from universal atrial coordinate (UAC) system mapped on to a representative LA model. (B) Beta coordinate from UAC mapped on to a representative LA model. (C) 2D representation of UAC with pulmonary vein locations labeled. Dashed lines represent edges of the five atrial regions. (D) Segmented LA mapped onto a 3D mesh with numbered regions corresponding to regions in (C). (E) Final division scheme after edge expansion of the LPVs and RPVs to generate regions 3 and 4 respectively.

Supplemental Video 1. Dynamic illustration of reentrant arrhythmia sustained by dual simultaneous RDs. The video shows membrane voltage over time for the same episode of induced arrhythmia highlighted in Fig. 5 and discussed in the main text.